In A. Kuijper, T. Pock, K. Bredies, H. Bischof, eds., Scale Space and Variational Methods in Computer Vision, Lecture Notes in Computer Science, vol. 7893, pp. 392–403,


# Relations between Amoeba Median Algorithms and Curvature-Based PDEs

Martin Welk

University for Health Sciences, Medical Informatics and Technology (UMIT),
Eduard-Wallnöfer-Zentrum 1, 6060 Hall/Tyrol, Austria
martin.welk@umit.at

**Abstract.** This paper is concerned with the theoretical analysis of structure-adaptive median filter algorithms that approximate curvature-based PDEs for image filtering and segmentation. These so-called morphological amoeba filters, introduced by Lerallut et al. and further developped by Welk et al., achieve similar results as the well-known geodesic active contour and self-snakes PDEs. In the present work, the PDE approximated by amoeba active contours is derived in the general case. This PDE is structurally similar but not identical to the geodesic active contour equation. Implications for the qualitative behaviour of amoeba active contours as well as for the approximation of the pre-smoothed self-snakes equation are investigated.

## 1 Introduction

Introduced by Lerallut et al. [11, 12], morphological amoeba filtering is a class of discrete image filtering procedures based on image-adaptive structuring elements. These structuring elements are defined by a so-called amoeba metric that combines spatial proximity and grey-value similarity. Amoeba filters adapt flexibly to image structures. For example, iterated *amoeba median filtering* (AMF) improves the favourable edge-preserving denoising capabilities of traditional iterated median filtering [17] by removing its tendency to dislocate edges, and introducing even edge-enhancing behaviour.

Extending the author's earlier work with co-authors [18, 19], this paper is concerned with comparing AMF methods to two curvature-based PDEs of image processing. Firstly, we consider *geodesic active contours* [3, 4, 8, 9]

$$u_t = |\nabla u| \operatorname{div}\left(g(|\nabla f|^2)\,\frac{\nabla u}{|\nabla u|}\right) \tag{1}$$

which can be used to segment a given image $f$ by evolving a contour towards regions of high contrast in $f$. The evolving contour is encoded as zero-level set of the function $u$. The (decreasing, nonnegative) edge-stopping function $g$ can be chosen e.g. as a Perona-Malik-type function [15]

$$g(s^2) = \frac{1}{1+s^2/\lambda^2}\,, \qquad \lambda > 0\,. \tag{2}$$

Secondly, we are interested in *self-snakes* [16], a PDE filter for a single image $u$ that is obtained from (1) by identifying $f$ with the evolving function $u$.

As shown in [19], AMF is linked to the self-snakes equation in a way similar to the connection of traditional median filtering to (mean) curvature motion [1] that was proven by Guichard and Morel [6]: One amoeba median filtering step asymptotically approximates a time step of size $\varrho^2/6$ of an explicit time discretisation for the self-snakes PDE when the radius $\varrho$ of the structuring element goes to zero. The exact shape of the (decreasing, nonnegative) edge-stopping function $g$ depends on the specific choice of the amoeba metric, with the Perona-Malik-type function (2) being associated to the $L^2$ amoeba metric.

Building on this amoeba/self-snakes connection, [18] proposed a morphological amoeba algorithm for active contour segmentation. Experimentally, this process behaves similar to geodesic active contours, with a tendency to refined adaptation to structure details, see [18, Fig. 2]. Analysis in [18] was restricted to a rotationally symmetric situation where asymptotic equivalence to geodesic active contours (1) could be proven. The present paper aims at closing this gap in theoretical analysis.

Writing the self-snakes equation ((1) with $f \equiv u$) as $u_t = g\cdot|\boldsymbol{\nabla} u|\,\mathrm{div}(\boldsymbol{\nabla} u/|\boldsymbol{\nabla} u|)+ \langle\boldsymbol{\nabla} g, \boldsymbol{\nabla} u\rangle$ accentuates an important difference between the (mean) curvature motion equation $u_t = |\boldsymbol{\nabla} u|\,\mathrm{div}(\boldsymbol{\nabla} u/|\boldsymbol{\nabla} u|)$ and self-snakes: the edge-enhancing component $\langle\boldsymbol{\nabla} g, \boldsymbol{\nabla} u\rangle$ is related to a shock filter [14, 16] or backward diffusion [16]. Analytically, this makes the self-snakes PDE ill-posed, and in particular induces staircasing behaviour [20]. Numerically, this shock component needs specific consideration. In finite-difference discretisations, it is usually treated by an upwind discretisation [13]. Still, severe numerical dissipation artifacts appear. As [19] demonstrates, results depend heavily on the grid mesh size, rendering the approximation of the PDE unreliable.

One approach to defeat these undesired phenomena on the PDE level itself, and to construct a PDE that can properly be numerically approximated, is pre-smoothing [5]. To this end, one replaces $\boldsymbol{\nabla} u$ in the argument of $g$ by a smoothed version like $\boldsymbol{\nabla} u_\sigma := K_\sigma * \boldsymbol{\nabla} u$ where $K_\sigma$ denotes a Gaussian of standard deviation $\sigma$.

As [19] suggests, AMF can be considered as an unconventional discretisation of self-snakes. Experiments in [19] indicate that it is less susceptible to the above-mentioned sort of artifacts. This indicates that the AMF procedure also acts in some way regularising. To make a first step towards a better understanding of the regularisation effects of pre-smoothing and amoeba filtering is another objective of this work.

**Our contribution.** We extend the analytical investigation of amoeba filters. First, we derive the PDE corresponding to the amoeba active contour method in the general case, which is no longer fully identical to the geodesic active contour equation. To this end, we introduce a proof strategy substantially different from that used in [18, 19]. Qualitative differences between geodesic and amoeba active contours are discussed based on the approximation result.

Finally, we apply our extended analysis of amoeba active contours to amoeba approximation of pre-smoothed self-snakes.

**Structure of the paper.** We give a short account of the basic concepts of amoeba filtering in Section 2. Our main theoretical result on PDE approximation is proven in

Section 3. It is used for comparing amoeba active contours to geodesic active contours in Section 4. Pre-smoothing in the self-snakes PDE and its approximation in the amoeba framework is discussed in Section 5, followed by a conclusion in Section 6.

## 2 Amoeba Filters

In this section we recall shortly the definition of amoeba metrics and amoeba filters. We assume that a 2D image is given as a smooth function $f : \Omega \to \mathbb{R}$ where $\Omega \subset \mathbb{R}^2$ is closed.

**Amoeba metrics.** Following the spatially continuous formulation of the amoeba framework in [18, 19], we associate with $f$ the image manifold $\Gamma \subset \mathbb{R}^3$ consisting of the points $(x, y, \beta f(x, y))$. As a Riemannian metric on $\Gamma$, an *amoeba metric* is given by

$$\mathrm{d}_\nu s = \nu\left(\sqrt{\mathrm{d}x^2 + \mathrm{d}y^2}, \beta\, \mathrm{d}f\right) , \tag{3}$$

where $\nu$ is some norm on $\mathbb{R}^2$. The use of the Euclidean norm $\sqrt{\mathrm{d}x^2 + \mathrm{d}y^2}$ in the spatial component ensures rotational invariance of the amoeba metric, while the combination of spatial and tonal distances is governed by $\nu$. The factor $\beta$ is a scale that balances the spatial and tonal information.

The *amoeba distance* $d(\boldsymbol{p}, \boldsymbol{q})$ between two points $\boldsymbol{p}$, $\boldsymbol{q}$ of the image domain is the minimum of $L(\boldsymbol{c}) = \int_{\boldsymbol{c}} \mathrm{d}_\nu s$ among all curves $\boldsymbol{c}$ connecting $\boldsymbol{p}$ with $\boldsymbol{q}$.

**Continuous-scale amoeba filtering formulation.** For amoeba filters, one defines a structuring element $\mathcal{A}_{\boldsymbol{p}}$ for each point $\boldsymbol{p} \in \Omega$ as the set of all $\boldsymbol{q} \in \Omega$ such that $d(\boldsymbol{p}, \boldsymbol{q}) \leq \varrho$, where the global parameter $\varrho$ is the *amoeba radius*. With the so defined structuring elements several morphological filters can be carried out straightforward. In particular, for amoeba median filtering (AMF), the median of the grey-values of the given image $f$ within $\mathcal{A}_{\boldsymbol{p}}$ becomes the filtered grey-value at $\boldsymbol{p}$. Like traditional median filtering, this filter can be applied iteratively. This process was studied in [19].

**Amoeba active contours.** The amoeba active contour method described in [18] acts in a similar way: Structuring elements are determined as before but on the basis of the given image $f$, and are used for median-filtering the evolving level-set function $u$.

**Discrete amoeba filtering algorithms.** Practically, computations are done on discrete images, using a discrete version of the above-mentioned amoeba distance obtained by restricting curves to paths in the neighbourhood graph of the image grid, either with 4-neighbourhoods as in [11, 12] or with 8-neighbourhoods as in [18, 19]. More sophisticated constructions using geometric distance transforms [2, 7] would be possible.

**Choice of the amoeba metric for the analysis.** In the following, we use the $L^2$ amoeba metric given by $\nu(s, t) = \sqrt{s^2 + t^2}$. The amoeba metric parameter $\beta$ can be fixed to 1 since a change of this parameter is equivalent to a simple rescaling of the steering function $f$.

## 3 Analysis of Amoeba Active Contours

We study an amoeba median filter for $\varrho \to 0$, in which $f$ is a smooth function from which the amoeba structuring elements are generated, and $u$ is another smooth function, to which the median filter is applied. In our analysis, local orthonormal bases aligned to the gradient and level-line directions of both functions will play an important role. Given a location $\boldsymbol{x}_0$ in the image domain, we will therefore denote by $\boldsymbol{\chi} = (\cos\varphi, \sin\varphi)^{\mathrm{T}}$ the normalised gradient vector of $f$ at $\boldsymbol{x}_0$. The unit vector $\boldsymbol{\zeta} \perp \boldsymbol{\chi}$ then indicates the local level line direction of $f$. Analogously, we denote by $\boldsymbol{\eta}$ a normalised gradient vector for $u$, and by $\boldsymbol{\xi} \perp \boldsymbol{\eta}$ the unit vector in the level line direction. The angle between the gradient directions will be called $\alpha$, such that $\boldsymbol{\eta} = \bigl(\cos(\varphi+\alpha), \sin(\varphi+\alpha)\bigr)^{\mathrm{T}}$. We will prove the following fact.

**Theorem 1.** *One step of amoeba median filtering of a smooth function $u$ governed by amoebas generated from $f$ with an amoeba radius of $\varrho$ asymptotically approximates a time step of size $\tau = \varrho^2/6$ of an explicit time discretisation for the PDE*

$$u_t = \frac{u_{\boldsymbol{\xi}\boldsymbol{\xi}}}{1 + |\boldsymbol{\nabla} f|^2 \sin^2\alpha} - \frac{|\boldsymbol{\nabla} f|\,|\boldsymbol{\nabla} u|}{1 + |\boldsymbol{\nabla} f|^2 \sin^2\alpha} \cdot \left( \frac{f_{\boldsymbol{\zeta}\boldsymbol{\zeta}} \cos^3\alpha}{1 + |\boldsymbol{\nabla} f|^2} + 2\, f_{\boldsymbol{\zeta}\boldsymbol{\chi}} \sin^3\alpha + \frac{f_{\boldsymbol{\chi}\boldsymbol{\chi}} \cos\alpha \bigl(2 + \sin^2\alpha + 3\,|\boldsymbol{\nabla} f|^2 \sin^2\alpha\bigr)}{\bigl(1 + |\boldsymbol{\nabla} f|^2\bigr)^2} \right). \quad (4)$$

**Remark on the proof strategy.** The proofs in [18, 19] were based on measuring level line segments within the amoeba. Throughout the proofs, Taylor coefficients of $f$ and $u$ up to second order were used in the calculations. This strategy could be followed in the more specialised cases treated in those papers. However, the complexity of such calculations would increase a lot in the general case we are about to discuss. In the following proof of the theorem we follow therefore a different strategy that measures areas not segments but sectors of amoebas via a polar coordinate representation. Level lines other than the one through the amoeba centre are not considered directly any more.

**Finding the amoeba contour.** To determine the shape of the amoeba $\mathcal{A} := \mathcal{A}_{\boldsymbol{x}_0}$ around a point $\boldsymbol{x}_0 \in \Omega$, we start by considering the 1D case: given $f : \mathbb{R} \to \mathbb{R}$, we seek $z_\pm \in \mathbb{R}$ such that the arc-length of the image graph of $f$ between $x_0$ and each of $x_0 + z_+$, $x_0 - z_-$ equals $\varrho$. Certainly, $z_\pm \le \varrho$.

Using Taylor expansions for $f$ and the square root function, we have for the arc-length from $x_0$ to $x_0 + z$ (where $z > 0$)

$$\int_{x_0}^{x_0+z} \sqrt{1 + f'(x)^2}\,\mathrm{d}x = z\,\sqrt{1 + f'(x_0)^2} + \frac{z^2}{2}\,\frac{f'(x_0)\,f''(x_0)}{\sqrt{1 + f'(x_0)^2}} + \mathcal{O}(\varrho^3)\,. \quad (5)$$

Equating this to $\varrho$ yields a quadratic equation in $z$ with the solutions

$$z_{1,2} = \frac{1 + f'(x_0)^2}{f'(x_0)\,f''(x_0)} \left( -1 \pm \sqrt{1 + \varrho\,\frac{f'(x_0)\,f''(x_0)}{\bigl(1 + f'(x_0)\bigr)^{3/2}}} \right) + \mathcal{O}(\varrho^3) \quad (6)$$

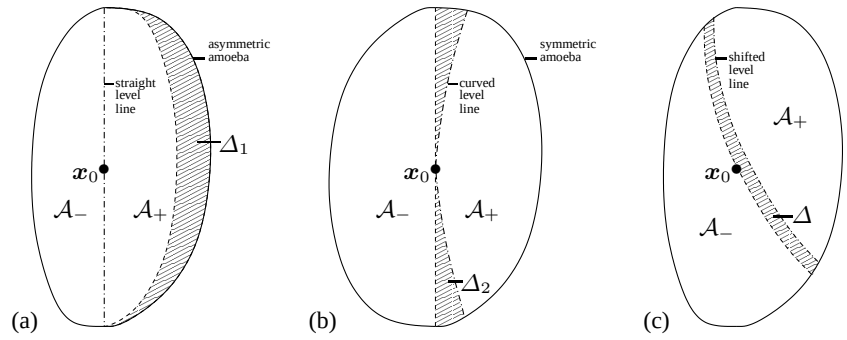


**Fig. 1. Left to right: (a)** Area difference $\Delta_1$ in an asymmetric amoeba with straight level lines. – **(b)** Area difference $\Delta_2$ in a symmetric amoeba with curved level lines. – **(c)** Compensation of the area difference $\Delta$ by shifting the central level line (schematic).

which gives $z_+$ as the "+" case (because of $z > 0$). Using again the Taylor expansion of the square root function, and doing an analogous derivation for $z_-$, we arrive at

$$z_\pm = \frac{\varrho}{\sqrt{1 + f'(x_0)^2}} \mp \frac{\varrho^2 \, f'(x_0) \, f''(x_0)}{2\big(1 + f'(x_0)^2\big)^2} + \mathcal{O}(\varrho^3) \, . \tag{7}$$

Turning to the 2D case, we approximate each shortest path in the amoeba metric from $\boldsymbol{x}_0$ to a point on the amoeba contour by a Euclidean straight line in the image plane. This introduces only an $\mathcal{O}(\varrho^3)$ error for the path length. We consider now the straight line through $\boldsymbol{x}_0$ in the direction of a given unit vector $\boldsymbol{v} \in \mathbb{R}^2$. By our previous 1D result, with the directional derivatives $f_{\boldsymbol{v}}(\boldsymbol{x}_0) = \langle \boldsymbol{v}, \boldsymbol{\nabla} f(\boldsymbol{x}_0) \rangle$ and $f_{\boldsymbol{vv}}(\boldsymbol{x}_0) = \boldsymbol{v}^{\mathrm{T}} \, \mathrm{D}^2 f(\boldsymbol{x}_0) \, \boldsymbol{v}$, we see that said straight line intersects the amoeba contour at $\boldsymbol{x}_0 \pm z_\pm(\boldsymbol{v}) \cdot \boldsymbol{v}$ with

$$z_\pm(\boldsymbol{v}) = \frac{\varrho}{\sqrt{1 + \big\langle \boldsymbol{v}, \boldsymbol{\nabla} f(\boldsymbol{x}_0) \big\rangle^2}} \mp \frac{\varrho^2 \, \big\langle \boldsymbol{v}, \boldsymbol{\nabla} f(\boldsymbol{x}_0) \big\rangle \, \boldsymbol{v}^{\mathrm{T}} \, \mathrm{D}^2 f(\boldsymbol{x}_0) \, \boldsymbol{v}}{2 \, \Big(1 + \big\langle \boldsymbol{v}, \boldsymbol{\nabla} f(\boldsymbol{x}_0) \big\rangle^2\Big)^2} + \mathcal{O}(\varrho^3) \, . \tag{8}$$

**Contributions to the amoeba median.** The median of $u$ within the structuring element $\mathcal{A}$ equals $u(\boldsymbol{x}_0)$ if (a) the amoeba is point-symmetric w.r.t. $\boldsymbol{x}_0$, and (b) the level lines of $u$ are straight: The central level line $u(\boldsymbol{x}) = u(\boldsymbol{x}_0)$ of $u$ then bisects $\mathcal{A}$, i.e. $\mathcal{A}_+ := \{\boldsymbol{x} \in \mathcal{A} \mid u(\boldsymbol{x}) \geq u(\boldsymbol{x}_0)\}$ and $\mathcal{A}_- := \{\boldsymbol{x} \in \mathcal{A} \mid u(\boldsymbol{x}) \leq u(\boldsymbol{x}_0)\}$ have equal area. For a similar bisection approach in a gradient descent for segmentation compare [10].

Deviations from conditions (a) and (b) lead to imbalances between $\mathcal{A}_+$ and $\mathcal{A}_-$. The median is determined by the shift of the central level line that is necessary to compensate for the resulting area difference. The separate area effects of asymmetry of the amoeba, and curvature of $u$'s level lines are of order $\mathcal{O}(\varrho^3)$, while any cross-effects are at least of order $\mathcal{O}(\varrho^4)$, and can be neglected for the purpose of our analysis. Therefore, the two effects can be studied independently.

*Asymmetry of the amoeba.* We start by analysing the effect of asymmetries of the point set $\mathcal{A}$, compare Figure 1(a). As the amoeba shape is governed by $f$, we will use the $\boldsymbol{\zeta}$,

$\boldsymbol{\chi}$ local coordinates. For an arbitrary unit vector $\boldsymbol{v} = \big(\cos(\varphi+\vartheta), \sin(\varphi+\vartheta)\big)^{\mathrm{T}}$ we have then

$$f_{\boldsymbol{v}}(\boldsymbol{x}_0) = |\boldsymbol{\nabla} f(\boldsymbol{x}_0)| \cos\vartheta \;, \tag{9}$$

$$\boldsymbol{v}^{\mathrm{T}}\, \mathrm{D}^2 f(\boldsymbol{x}_0)\, \boldsymbol{v} = f_{\boldsymbol{\zeta\zeta}} \sin^2\vartheta + 2\, f_{\boldsymbol{\zeta\chi}} \cos\vartheta\, \sin\vartheta + f_{\boldsymbol{\chi\chi}} \cos^2\vartheta \tag{10}$$

which can be inserted into (8) to obtain $z_\pm(\varphi+\vartheta) := z_\pm(\boldsymbol{v})$.

Assume now that $u$ has straight level lines; remember that $\varphi+\alpha$ is the direction angle of its gradient direction. Since the amoeba shape is given by $z_\pm(\boldsymbol{v})$ in polar coordinates, the sought area difference is then obtained as

$$\Delta_1 := |\mathcal{A}_+| - |\mathcal{A}_-| = \int\limits_{\varphi+\alpha-\pi/2}^{\varphi+\alpha+\pi/2} \big(z_+(\vartheta) - z_-(\vartheta)\big)\, \frac{z_+(\vartheta)+z_-(\vartheta)}{2}\, \mathrm{d}\vartheta + \mathcal{O}(\varrho^4) \;. \tag{11}$$

The integral on the right-hand side equals

$$-\varrho^3\, |\boldsymbol{\nabla} f| \int\limits_{\alpha-\pi/2}^{\alpha+\pi/2} \frac{f_{\boldsymbol{\zeta\zeta}}\, \cos\vartheta\, \sin^2\vartheta + 2\, f_{\boldsymbol{\zeta\chi}}\, \cos^2\vartheta\, \sin\vartheta + f_{\boldsymbol{\chi\chi}}\, \cos^3\vartheta}{\big(1+|\boldsymbol{\nabla} f|^2 \cos^2\vartheta\big)^{5/2}}\, \mathrm{d}\vartheta \tag{12}$$

which evaluates to

$$\begin{aligned} -\frac{2}{3}\, \varrho^3\, |\boldsymbol{\nabla} f| \Bigg( & \frac{f_{\boldsymbol{\zeta\zeta}}\, \cos^3\alpha}{\big(1+|\boldsymbol{\nabla} f|^2\big)\big(1+|\boldsymbol{\nabla} f|^2\, \sin^2\alpha\big)^{3/2}} + \frac{2\, f_{\boldsymbol{\zeta\chi}}\, \sin^3\alpha}{\big(1+|\boldsymbol{\nabla} f|^2\, \sin^2\alpha\big)^{3/2}} \\ & + \frac{f_{\boldsymbol{\chi\chi}}\, \cos\alpha\, \big(2+\sin^2\alpha+3\,|\boldsymbol{\nabla} f|^2\, \sin^2\alpha\big)}{\big(1+|\boldsymbol{\nabla} f|^2\big)^2\big(1+|\boldsymbol{\nabla} f|^2\, \sin^2\alpha\big)^{3/2}} \Bigg) \;. \end{aligned} \tag{13}$$

*Curvature of the level lines.* The second source of area imbalance between $\mathcal{A}_+$ and $\mathcal{A}_-$ is the curvature of the level line of $u$ through $\boldsymbol{x}_0$. Using the $\boldsymbol{\xi}$, $\boldsymbol{\eta}$ local coordinates pertaining to $u$, this curvature equals $u_{\boldsymbol{\xi\xi}}/(2|\boldsymbol{\nabla} u|)$. The resulting area difference is

$$\begin{aligned} \Delta_2 := |\mathcal{A}_+| - |\mathcal{A}_-| &= -2 \int\limits_{-z_-(\varphi+\alpha+\pi/2)}^{z_+(\varphi+\alpha+\pi/2)} -\frac{u_{\boldsymbol{\xi\xi}}}{2\,|\boldsymbol{\nabla} u|} z^2\, \mathrm{d}z + \mathcal{O}(\varrho^4) \\ &= \frac{2}{3}\, \frac{u_{\boldsymbol{\xi\xi}}}{|\boldsymbol{\nabla} u|}\, \frac{\varrho^3}{\big(1+|\boldsymbol{\nabla} f|^2\, \sin^2\alpha\big)^{3/2}} + \mathcal{O}(\varrho^4) \;. \end{aligned} \tag{14}$$

**Median calculation.** As the median $\mu$ of $u$ within $\mathcal{A}$ belongs to the level line of $u$ that bisects the area of the amoeba, the difference $\mu - u(\boldsymbol{x}_0)$ corresponds to a shift of the central level line that compensates the area difference $\Delta_1 + \Delta_2$. This compensation is obtained when

$$2\, \frac{\mu - u(\boldsymbol{x}_0)}{|\boldsymbol{\nabla} u|} \cdot \big(z_+(\varphi+\alpha+\pi/2) + z_-(\varphi+\alpha+\pi/2)\big) = \Delta_1 + \Delta_2 + \mathcal{O}(\varrho^4) \;, \tag{15}$$

which finally gives $\mu = u(\boldsymbol{x}_0) + (\varrho^2/6) \cdot u_t$ with $u_t$ given by (4) up to an error $\mathcal{O}(\varrho)$. This concludes the proof of Theorem 1.

**Special cases.** The following two statements reproduce the more specialised approximation results from [19] (in the case of the $L^2$ amoeba metric) and [18], respectively.

**Corollary 1.** *The amoeba median filter with $f \equiv u/\lambda$ approximates the self-snakes equation*

$$u_t = \frac{u_{\boldsymbol{\xi\xi}}}{1 + |\boldsymbol{\nabla} u|^2/\lambda^2} - \frac{2\, u_{\boldsymbol{\eta\eta}}\, |\boldsymbol{\nabla} u|^2}{\lambda^2 \left(1 + |\boldsymbol{\nabla} u|^2/\lambda^2\right)^2} = |\boldsymbol{\nabla} u| \operatorname{div} \left( \frac{1}{1 + |\boldsymbol{\nabla} u|^2/\lambda^2} \frac{\boldsymbol{\nabla} u}{|\boldsymbol{\nabla} u|} \right) \tag{16}$$

*in the sense of Theorem 1.*

**Corollary 2.** *If input image $f$ and evolving level-set image $u$ are rotationally symmetric with respect to the origin, amoeba median filtering approximates the geodesic active contour equation*

$$u_t = \frac{u_{\boldsymbol{\xi\xi}}}{1 + |\boldsymbol{\nabla} f|^2} - \frac{2\, f_{\boldsymbol{\eta\eta}}\, |\boldsymbol{\nabla} u|\, |\boldsymbol{\nabla} f|}{\left(1 + |\boldsymbol{\nabla} f|^2\right)^2} = |\boldsymbol{\nabla} u| \operatorname{div} \left( \frac{1}{1 + |\boldsymbol{\nabla} f|^2} \frac{\boldsymbol{\nabla} u}{|\boldsymbol{\nabla} u|} \right) \tag{17}$$

*in the sense of Theorem 1.*

In the case of Corollary 1, one observes that its hypothesis entails that the identities $\alpha = 0$, $\boldsymbol{\zeta} = \boldsymbol{\xi}$, and $\boldsymbol{\chi} = \boldsymbol{\eta}$ hold everywhere. For Corollary 2, the assumed rotational symmetry yields $\alpha = 0$, $\boldsymbol{\zeta} = \boldsymbol{\xi}$, $\boldsymbol{\chi} = \boldsymbol{\eta}$, $u_{\boldsymbol{\xi\eta}} \equiv f_{\boldsymbol{\xi\eta}} \equiv 0$, and $u_{\boldsymbol{\xi\xi}}/u_{\boldsymbol{\eta}} \equiv f_{\boldsymbol{\xi\xi}}/f_{\boldsymbol{\eta}}$. Substituting the respective sets of identities into (4) implies the corollaries.

## 4 Comparison to Geodesic Active Contours

In the general amoeba active contour setting, however, it is evident that equation (4) does not exactly coincide with (1). For a better understanding of the differences between both active contour methods, we consider further typical configurations.

**Homogeneous image gradients.** In flat image regions ($\boldsymbol{\nabla} f = \mathbf{0}$), geodesic active contours (1) as well as amoeba active contours evolve the level set function $u$ by curvature motion. Let us consider now an image region with a homogeneous non-zero gradient, $\boldsymbol{\nabla} f = \mathrm{const}$. In such a region, geodesic active contours still perform curvature motion, but with an evolution speed slowed down by the contrast-dependent factor $g(|\boldsymbol{\nabla} f|^2) = 1/(1 + |\boldsymbol{\nabla} f|^2)$. The amoeba-based PDE (4) in this case becomes

$$u_t = \frac{u_{\boldsymbol{\xi\xi}}}{1 + |\boldsymbol{\nabla} f|^2 \sin^2 \alpha}\,, \tag{18}$$

i.e. also a slowed-down curvature motion, but the evolution is slowed down the less, the more the level lines of $f$ and $u$ are aligned. This leads to a faster straightening of aligned contour segments, thereby boosting adaptation of $u$'s level lines to those of $f$, see the schematic representation in Figure 2(a).

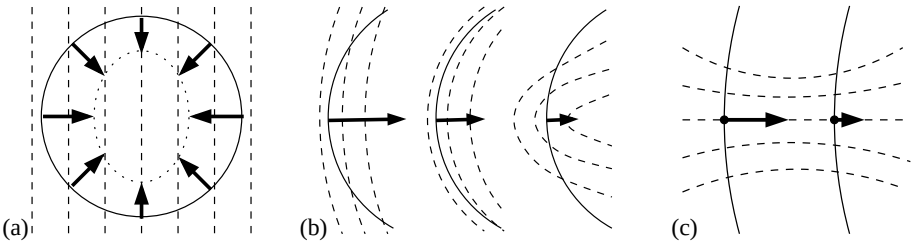


**Fig. 2.** Evolution of level lines under the PDE (4) in exemplary configurations (schematic). Solid lines: level lines of $u$, dashed lines: level lines of $f$. **Left to right: (a)** In a region with homogeneous $\boldsymbol{\nabla} f$, aligned level line segments of $u$ evolve faster. – **(b)** At a location with aligned $\boldsymbol{\nabla} u$ and $\boldsymbol{\nabla} f$, the contour evolves inward faster when the curvature of $u$ exceeds that of $f$. – **(c)** At locations with orthogonal $\boldsymbol{\nabla} u$ and $\boldsymbol{\nabla} f$, the curvature-dependent movement of the contour is attracted towards high-contrast regions of $f$. Assuming that $\boldsymbol{\eta}$ points to the right, $f_{\boldsymbol{\xi\eta}} < 0$ holds in the left, and $f_{\boldsymbol{\xi\eta}} > 0$ in the right part, while $u_{\boldsymbol{\xi\xi}} < 0$ in both cases.

**Aligned gradients.** Relaxing the condition of Corollary 2, we assume now that the gradient directions of $f$ and $u$ coincide, $\alpha = 0$, $\boldsymbol{\zeta} = \boldsymbol{\xi}$, $\boldsymbol{\chi} = \boldsymbol{\eta}$, but make no assumption on their curvatures. At such a location, (4) takes the form

$$\begin{aligned} u_t &= u_{\boldsymbol{\xi\xi}} - |\boldsymbol{\nabla} f|\,|\boldsymbol{\nabla} u| \left( \frac{f_{\boldsymbol{\xi\xi}}}{1+|\boldsymbol{\nabla} f|^2} + \frac{2\,f_{\boldsymbol{\eta\eta}}}{\left(1+|\boldsymbol{\nabla} f|^2\right)^2} \right) \\ &= \frac{u_{\boldsymbol{\xi\xi}}}{1+|\boldsymbol{\nabla} f|^2} - \frac{2\,|\boldsymbol{\nabla} f|\,|\boldsymbol{\nabla} u|\,f_{\boldsymbol{\eta\eta}}}{\left(1+|\boldsymbol{\nabla} f|^2\right)^2} + \frac{2\,|\boldsymbol{\nabla} f|^2\,|\boldsymbol{\nabla} u|}{1+|\boldsymbol{\nabla} f|^2} \left( \frac{u_{\boldsymbol{\xi\xi}}}{2\,u_{\boldsymbol{\eta}}} - \frac{f_{\boldsymbol{\xi\xi}}}{2\,f_{\boldsymbol{\eta}}} \right) \end{aligned} \tag{19}$$

which coincides with the corresponding geodesic active contour evolution except for the last summand that speeds up the evolution if the level line curvature $u_{\boldsymbol{\xi\xi}}/(2\,u_{\boldsymbol{\eta}})$ of $u$ exceeds that of $f$, see Figure 2(b). The same offset is obtained in the anti-aligned case, $\alpha = \pi$, $\boldsymbol{\zeta} = -\boldsymbol{\xi}$, $\boldsymbol{\chi} = -\boldsymbol{\eta}$; note that the curvature of $f$'s level lines is measured with respect to the orientation of $u$'s level lines. Relative to geodesic active contours, this implies an accelerated removal of sharp contour corners that do not match the given image $f$.

**Orthogonal gradients.** Consider now the complementary situation where the gradient directions of $u$ and $f$ are orthogonal, i.e. $\alpha = \pi/2$, $\boldsymbol{\zeta} = \boldsymbol{\eta}$, $\boldsymbol{\chi} = -\boldsymbol{\xi}$. Then (4) becomes

$$u_t = \frac{u_{\boldsymbol{\xi\xi}}}{1+|\boldsymbol{\nabla} f|^2} + \frac{2\,|\boldsymbol{\nabla} f|\,|\boldsymbol{\nabla} u|\,f_{\boldsymbol{\xi\eta}}}{1+|\boldsymbol{\nabla} f|^2} \tag{20}$$

where the last summand is by a factor $\left(1+|\boldsymbol{\nabla} f|^2\right)$ larger than in the corresponding geodesic active contour evolution. This means that attraction of the contour in $u$ towards high-contrast regions in $f$ is strengthened, see Figure 2(c).

In summary, our findings indicate that compared to geodesic active contours (1) the amoeba active contour equation (4) tends to attract the contour $u$ faster to high-contrast

image regions and to strengthen the alignment of level lines of $u$ to those of $f$. These effects are in line with the somewhat finer adaptation of amoeba active contours to structure details that was observed in [18].

## 5 Pre-smoothing and Amoeba Filters

The approximation result of [19], compare Corollary 1, refers to the self-snakes PDE (1) with $f \equiv u/\lambda$. As pointed out in the introduction, a disadvantage of this PDE is its ill-posedness that is often countered by pre-smoothing, i.e.

$$u_t = |\boldsymbol{\nabla} u| \operatorname{div}\left( g(|\boldsymbol{\nabla} u_\sigma|^2) \frac{\boldsymbol{\nabla} u}{|\boldsymbol{\nabla} u|} \right) \tag{21}$$

with $u_\sigma = K_\sigma * u$.

This procedure can be translated in a straightforward way to our amoeba median filter setting. One only needs to carve the amoeba structuring elements based on the pre-smoothed image $u_\sigma$ instead of $u$. The resulting filtering step is described by our amoeba active contour model with $f \equiv u_\sigma/\lambda$, such that the approximation result from Theorem 1 applies. Analogous to our discussion in the amoeba active contour setting this means that in the limit $\varrho \to 0$ not exactly (21) is approximated but a self-snakes equation with a modified pre-smoothing.

However, in practical computation of amoeba filters one always uses a positive amoeba radius $\varrho$. This means that such a filtering procedure with amoebas derived from $f = u_\sigma/\lambda$ would contain two spatial scale parameters, $\sigma$ and $\varrho$, both of which act as some sort of spatial averaging.

It can therefore be conjectured that the amoeba radius itself acts similarly as a pre-smoothing step. While a more exhausting investigation of this issue has to be left for future work, we compare pre-smoothed self-snakes with $g(s^2) = 1/(1+s^2)$ to amoeba median filtering ($f = u$) with positive amoeba radius for a very simple example.

**Test case.** We consider the function $u : \mathbb{R}^2 \to \mathbb{R}$ given by

$$u(x, y) = x + \varepsilon \cos(kx) , \qquad \varepsilon \ll 1 . \tag{22}$$

It is composed of a simple linear slope (which would be stationary under each of the filters) and single-frequency perturbations of small amplitude. We will analyse the response of filters to that perturbation, dependent on the frequency parameter $k$.

Given the nonlinearity of the filters in question, there is no superposition property for these perturbations. Nevertheless, sufficiently small perturbations will interact with each other only in higher order terms $\mathcal{O}(\varepsilon^2)$, such that the technique will still give some intuition of the behaviour of the filters.

The chosen setting is representative of the practically meaningful situation of staircasing arising in a smooth transition.

**Self-snakes.** In our test case all level lines are parallel, so the 2D self-snakes equation simplifies to $u_t = g\,|\boldsymbol{\nabla} u|\,\operatorname{div}\bigl(\boldsymbol{\nabla} u/|\boldsymbol{\nabla} u|\bigr) + \langle \boldsymbol{\nabla} g, \boldsymbol{\nabla} u\rangle$. The first summand vanishes, while the second one simplifies to $g_x u_x$. From (22) we obtain $u_x = 1 - \varepsilon\, k\, \sin(kx)$, and with $g$ as given by (2) further $g_x = \frac{1}{2}\,\varepsilon\, k^2\, \cos(kx) + \mathcal{O}(\varepsilon^2)$. Thus, we have

$$u_t = g_x u_x = \frac{\varepsilon\, k^2}{2}\, \cos(kx) + \mathcal{O}(\varepsilon^2) \tag{23}$$

indicating an indefinite amplification of higher frequencies. At the same time, the higher-order terms resulting from nonlinearity lead to an instantaneous propagation of the perturbation from a given frequency $k$ to higher frequencies, which means that even for a single-frequency perturbation arbitrarily high frequencies with arbitrarily high amplification ratios will appear within short evolution time, enabling a loss of regularity of the evolving function.

*Pre-smoothing.* Replacing $g \equiv g(|\boldsymbol{\nabla} u|^2)$ with $g_\sigma \equiv g(|\boldsymbol{\nabla} u_\sigma|^2)$, we have in our test case $u_\sigma = x + \varepsilon\, \mathrm{e}^{-k^2\sigma^2/2} \cos(kx)$, thus $\partial_x g_\sigma = \frac{\varepsilon\, k^2}{2}\, \mathrm{e}^{-k^2\sigma^2/2} \cos(kx) + \mathcal{O}(\varepsilon^2)$ and finally

$$u_t = \partial_x g_\sigma \cdot \partial_x u = \frac{\varepsilon\, k^2}{2}\, \mathrm{e}^{-k^2\sigma^2/2} \cos(kx) + \mathcal{O}(\varepsilon^2)\ . \tag{24}$$

Unlike before, the amplification ratio $k^2 \exp(-k^2\sigma^2/2)$ is bounded and reaches a maximum for $k = \sqrt{2}/\sigma$, such that regularity of the evolving function is kept.

**Amoeba filter with finite-size radius.** We calculate the effect of amoeba median filtering with amoeba radius $\varrho$ on our test case in the same way as in the proof of Theorem 1 via the area difference $\Delta := |\mathcal{A}_1| - |\mathcal{A}_2|$. As in our test settings level lines are not curved, only the asymmetry contribution $\Delta_1$ needs to be considered.

The amoeba around $\boldsymbol{x}_0 = (x_0, y_0)$ is symmetric with respect to the line $y = y_0$ (parallel to the $x$-axis). We parametrise this symmetry line as $(x(s), y_0)$, where $s$ is an arc-length parameter in the amoeba metric, i.e.

$$\int_0^{x(s)} \sqrt{1 + u_x^2(z, y_0)}\, \mathrm{d}z = s\ . \tag{25}$$

From the level line through $(x(s), y_0)$ (parallel to the $y$-axis), the amoeba cuts out a piece of length $2\sqrt{\varrho^2 - s^2}$. The sought area difference is therefore

$$\begin{aligned}\Delta(\boldsymbol{x}_0) &= \int_0^{\varrho} \frac{2\sqrt{\varrho^2 - s^2}}{\sqrt{1 + u_x^2(x(s), y_0)}}\, \mathrm{d}s - \int_{-\varrho}^{0} \frac{2\sqrt{\varrho^2 - s^2}}{\sqrt{1 + u_x^2(x(s), y_0)}}\, \mathrm{d}s \\ &= 2\int_0^{\varrho} \sqrt{\varrho^2 - s^2} \left( \frac{1}{\sqrt{1 + u_x^2(x(s), y_0)}} - \frac{1}{\sqrt{1 + u_x^2(x(-s), y_0)}} \right) \mathrm{d}s \end{aligned} \tag{26}$$

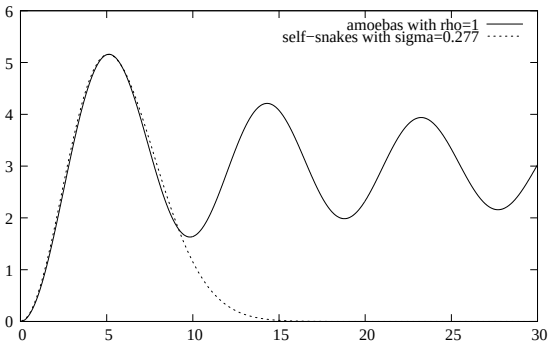


**Fig. 3.** Comparison of amplification factors depending on the frequency parameter $k$ for pre-smoothed self-snakes and amoeba median filtering with fixed amoeba size. Horizontal axis shows $k$, vertical axis shows amplification factors.

with $u_x(x, y) = 1 - k\,\varepsilon\,\sin(k\,x)$.

Analogously to (15), the resulting median is $u(\boldsymbol{x}_0) + \Delta(\boldsymbol{x}_0)/(4\,\varrho)$. Numerical integration of (26) confirms that $\Delta(x, y_0)$ itself is approximately a multiple of the perturbation function $\varepsilon\,\cos(k\,x)$. For easy comparison with (24), we divide the amplification factor $\Delta(x, y_0)/(4\,\varrho\,\cos(k\,x))$ by $\varrho^2/6$ (the evolution time corresponding to amoeba radius $\varrho$ in the asymptotic approximation results).

Figure 3 shows the numerically computed factor $\Delta(x, y_0)/(4\,\varrho\,\cos(k\,x)) \cdot 6/\varrho^2$ along with the factor $k^2\exp(-k^2\sigma^2/2)/2$ from (24) as functions of the frequency parameter $k$. Here, $\varrho$ and $\sigma$ were chosen for an optimal fit of the first maximum. It is evident that the first lobe of the amplification functions is very similar. For higher frequencies the exponential dampening of the pre-smoothed self-snakes is superior to the oscillations of the amoeba amplification factor around a positive value. However, when practically filtering images, higher frequencies are cut off by spatial discretisation anyway. If the amoeba radius is not larger than approx. $10/\pi \approx 3$, the higher lobes of the amplification function in Figure 3 will disappear entirely.

## 6 Conclusion

We have analysed our amoeba active contour method proposed in [18] and derived a partial differential equation that it approximates asymptotically for vanishing structuring element size. Our result reproduces as special cases two earlier results from literature: the approximation of geodesic active contours in a special case [18] and the approximation of self-snakes by iterated amoeba median filtering [19]. In the general case, the PDE derived here differs from the geodesic active contour equation. The implications of the differences for active contour segmentation have been discussed and found to be consistent with the experimental findings of [18].

Finally, we have discussed from the same view point the approximation of self-snakes with pre-smoothing by amoeba filters. As a first step towards a more comprehensive investigation of the relation between curvature-based PDEs with pre-smoothing, and amoeba filtering with non-vanishing structuring elements, we have compared the effect of both methods in a simple special case with single-frequency perturbations of a constant gradient image. Future work extending this analysis is expected to lead to a deeper understanding of the interplay between adaptive morphology and PDE methods.

## References


1. Alvarez, L., Lions, P.L., Morel, J.M.: Image selective smoothing and edge detection by nonlinear diffusion. II. SIAM Journal on Numerical Analysis **29** (1992) 845–866
2. Borgefors, G.: Distance transformations in digital images. Computer Vision, Graphics and Image Processing **34** (1986) 344–371
3. Caselles, V., Kimmel, R., Sapiro, G.: Geodesic active contours. In: Proc. Fifth International Conference on Computer Vision, Cambridge, MA, IEEE Computer Society Press (June 1995) 694–699
4. Caselles, V., Kimmel, R., Sapiro, G.: Geodesic active contours. International Journal of Computer Vision **22** (1997) 61–79
5. Feddern, C., Weickert, J., Burgeth, B., Welk, M.: Curvature-driven PDE methods for matrix-valued images. International Journal of Computer Vision **69**(1) (August 2006) 91–103
6. Guichard, F., Morel, J.M.: Partial differential equations and image iterative filtering. In Duff, I.S., Watson, G.A., eds.: The State of the Art in Numerical Analysis. Number 63 in IMA Conference Series (New Series). Clarendon Press, Oxford (1997) 525–562
7. Ikonen, L., Toivanen, P.: Shortest routes on varying height surfaces using gray-level distance transforms. Image and Vision Computing **23**(2) (2005) 133–141
8. Kichenassamy, S., Kumar, A., Olver, P., Tannenbaum, A., Yezzi, A.: Gradient flows and geometric active contour models. In: Proc. Fifth International Conference on Computer Vision, Cambridge, MA, IEEE Computer Society Press (June 1995) 810–815
9. Kichenassamy, S., Kumar, A., Olver, P., Tannenbaum, A., Yezzi, A.: Conformal curvature flows: from phase transitions to active vision. Archives for Rational Mechanics and Analysis **134** (1996) 275–301
10. Kimmel, R.: Fast edge integration. In Osher, S., Paragios, N., eds.: Geometric Level Set Methods in Imaging, Vision and Graphics. Springer, New York (2003) 59–77
11. Lerallut, R., Decencière, E., Meyer, F.: Image processing using morphological amoebas. In Ronse, C., Najman, L., Decencière, E., eds.: Mathematical Morphology: 40 Years On. Volume 30 of Computational Imaging and Vision. Springer, Dordrecht (2005)
12. Lerallut, R., Decencière, E., Meyer, F.: Image filtering using morphological amoebas. Image and Vision Computing **25**(4) (2007) 395–404
13. Osher, S., Sethian, J.A.: Fronts propagating with curvature-dependent speed: Algorithms based on Hamilton–Jacobi formulations. Journal of Computational Physics **79** (1988) 12–49
14. Osher, S., Rudin, L.I.: Feature-oriented image enhancement using shock filters. SIAM Journal on Numerical Analysis **27** (1990) 919–940
15. Perona, P., Malik, J.: Scale space and edge detection using anisotropic diffusion. IEEE Transactions on Pattern Analysis and Machine Intelligence **12** (1990) 629–639
16. Sapiro, G.: Vector (self) snakes: a geometric framework for color, texture and multiscale image segmentation. In: Proc. 1996 IEEE International Conference on Image Processing. Volume 1., Lausanne, Switzerland (September 1996) 817–820
17. Tukey, J.W.: Exploratory Data Analysis. Addison–Wesley, Menlo Park (1971)
18. Welk, M.: Amoeba active contours. In Bruckstein, A.M., ter Haar Romeny, B., Bronstein, A.M., Bronstein, M.M., eds.: Scale Space and Variational Methods in Computer Vision. Volume 6667 of Lecture Notes in Computer Science. Springer, Berlin (2012) 374–385
19. Welk, M., Breuß, M., Vogel, O.: Morphological amoebas are self-snakes. Journal of Mathematical Imaging and Vision **39** (2011) 87–99
20. You, Y.L., Kaveh, M., Xu, W., Tannenbaum, A.: Analysis and design of anisotropic diffusion for image processing. In: Proc. 1994 IEEE International Conference on Image Processing. Volume 2., Austin, Texas, USA (November 1994) 497–501